

Surviving Wireless Energy Interference in RF-harvesting Sensor Networks: An Empirical Study

M. Yousof Naderi,^{*} Kaushik R. Chowdhury,^{*} Stefano Basagni,^{*}
Wendi Heinzelman,[†] Swades De,[‡] and Soumya Jana[§]

^{*}Department of Electrical and Computer Engineering, Northeastern University, Boston, MA, U.S.A
E-mail: {naderi, krc, basagni}@ece.neu.edu

[†]Department of Electrical and Computer Engineering, University of Rochester, Rochester, NY, U.S.A
E-mail: wheinzel@ece.rochester.edu

[‡] Department of Electrical Engineering, IIT Delhi, New Delhi, India. E-mail: swadesd@ee.iitdernet.in

[§]Department of Electrical Engineering, IIT Hyderabad, Hyderabad, India. E-mail: jana@iith.ac.in

Abstract—Energy transfer through radio frequency (RF) waves enables battery-free operation for wireless sensor networks, while adversely impacting data communication. Thus, extending the lifetime for RF powered sensors comes at a cost of interference and reduced data throughput. This paper undertakes a systematic experimental study for both indoor and outdoor environments to quantify these tradeoffs. We demonstrate how separating the energy and data transfer frequencies gives rise to black (high loss), gray (moderate loss), and white (low loss) regions with respect to packet errors. We also measure the effect of the physical location of energy transmitters (ETs) and the impact of the spatial distribution of received interference power from the ETs, when these high power transmitters also charge the network. Our findings suggests leveraging the level of energy interference detected at the sensor node as a guiding metric to decide how best to separate the charging and communication functions in the frequency domain, as well as separating multiple ETs with slightly different center frequencies.

I. INTRODUCTION

Recent advancements in energy harvesting and wireless energy transfer through radio frequency (RF) waves have opened up new possibilities for powering the nodes of a wireless sensor network (WSN) wirelessly. This not only extends the network lifetime, but also obviates the problem of retrieving sensors and physically replacing batteries. The RF energy harvesting sensors convert the energy contained in incident electromagnetic radiation emitted by wireless energy transmitters (ETs) into stored electrical charge within a capacitor or re-chargeable battery. This limited stored energy can then be used for sensing, processing and communication. However, the high power of RF waves emitted from ETs interfere with low-power data communications among sensor nodes. This leads to interference and packet loss. The objective of this experimental study is to quantify this loss under various placements of ETs, including choice of frequencies and separation distances.

Motivation. The Federal Communications Commission

(FCC) permits up to 4 Watts effective isotropic radiated power (EIRP) for wireless energy transfer. Most Commercial Off-The-Shelf (COTS) ETs (e.g., Powercaster [1]) generate 3 Watts energy waves. These high levels of radiation are much higher than those of typical sensors, such as the MicaZ, whose maximum transmission power is limited to 1mW. Thus, the adverse impact of continuous RF energy transfer on sensor communication should be quantified. One approach could be using duty-cycle based energy and data transfer, resulting in controlled and pre-decided trade-offs between data throughput and energy harvesting levels [2]. At the hardware level, the state-of-the-art RF energy harvesting circuits can operate over a range of frequencies [3], [4]. Thus, if the ET frequencies can be separated from data frequencies then the packet losses caused by simultaneous data and energy transfer may be minimized. Previous empirical studies in WSNs have focused on understanding the coexistence between WSNs and WiFi [5], [6], microwave ovens [7], and smart grids [8]. There are also experimental studies on concurrent data transmissions on low-power wireless links [9], [10]. However, none of them have studied the interference issues in WSNs with wireless energy transfer. Moreover, the power difference between interfered signals (i.e. high power energy signal and low-power data) in RF-harvesting sensor networks is much higher than those in the previous studies, which necessitates to study the adjacent-channel interference of energy signals on low-power data communications in practice. To fill these gaps, this study is looking to find what are the observable impacts of energy interference, how to survive such interference, and leverage the interference level at each node for reliable data and energy transfer.

Experimental methodology. We conduct a series of experiments at indoor and outdoor locations to study the effects of (i) RF energy interference on data communication, (ii) the benefits of energy transfer when spread over different frequencies (i.e., under various separation levels of energy

and data frequencies), and (iii) the location of ETs on packet delivery. We present the distributions of energy interference measured by sensor nodes for different energy frequencies. Our experiments involve both statistical and time-trace measurements of packet reception rates, as well as the received interferer power under carefully-designed conditions. We use Mica2 motes and RF frequency-tunable ETs. To the best of our knowledge, this is the first empirical study on RF energy harvesting sensor networks.

Summary of findings. Our measurements indicate the presence of hard separation thresholds in the frequency domain that guarantee successful data packet reception among sensor nodes when ETs are transferring energy. This threshold changes with indoor/outdoor locations and separation distance of the ETs from the sensors. We identify three regions based on the separation of the energy and data transfer channels on the frequency scale, which we name as *black*, *gray*, and *white*, with high, moderate and low packet error rates, respectively. For example, the packet reception rate (PRR) when the ET transfers energy in the *gray* region can vary significantly with high temporal fluctuations. Also, sensors do not receive any packets in the *black* frequency region. However, wireless energy transfer at any *white* band of frequencies result in higher than 90% PRR. We find differing behavior in indoor and outdoor environments. For example, when RF transfer is done in the *gray* frequencies with increasing ET distance outdoor, the PRR improves monotonically. However, in indoor spaces, as ET increases, PRR has fluctuations due to signal reflections. On the contrary, when ET transfers at *white* frequencies, the PRR is almost the same in both indoor and outdoor experiments, regardless of ET locations. Finally, we find the interferer power at the sensor node that can be used to detect the frequency regions and set the appropriate energy transfer frequencies of ETs.

The rest of the paper is organized as follows. In Section II we describe our experimental methodology. Section III presents measurement results on packet reception performance, including the effect of multifrequency wireless energy transfer and the placement of the ET. Results on the distribution of received energy interference are discussed in Section IV. Section V presents the temporal variability of the energy interferer power. Section VI concludes the paper.

II. EXPERIMENTAL PLATFORM AND METHODOLOGY

A. Hardware and software

We use Mica2 motes as the data communicating and energy harvesting nodes. Each mote is equipped with CC1000 radio operating at 915 MHz with a default RF transmission power of 0 dBm. The receiving sensitivity is -98 dBm. The CC1000 radio supports the measurements of the received signal strength (RSSI). We link the P2110 RF energy harvesters from Powercast Co. [1] to the mote. The RF frequency-tunable wireless ET is an Agilent N5181 MXG RF signal generator connected to an amplifier with a 50Ω omnidirectional antenna and 3 W output power in

the 902–928 MHz band. This configurable ET setup lets us change the frequency of wireless energy transfer precisely.

B. Measurement Metrics

We use interference power and PRR as the measurement metrics. The PRR is the fraction of packets that are received within a time window over the total transmitted packets. We use a total of 360 packet transmission epochs to estimate the PRR with a precision of 1.2% for each particular combination of energy transmission frequency and distance between the ET and the motes. For each ET energy frequency, the motes take 600 RSSI samples at the rate of 10 samples/sec over the data channel (i.e., 915 MHz) that is important in a node’s point of view. Six hundred RSSI samples are enough to collect meaningful measurements about the level of energy interference on the data channel.

C. Locations

We conduct our experiments in indoor and outdoor environments. For the indoor environment we select a space with four plain walls and no other intermediate reflective objects to limit time-varying changes in the wireless channel due to multi-path fading and shadowing. The second set of measurements are conducted in an open-space outdoor, with no structural obstructions. Each experiment involves three nodes: The sender, the receiver, and the wireless ET. The motes and ET are placed on a flat table, 0.5 m from the floor. The sender and receiver nodes are placed one meter from each other, and they are equidistant from the ET. The locations of the sender and receiver sensor nodes are fixed, but we vary the frequency and distance of the ET and measure the packet reception rate and the relative interference experienced by the sensor motes.

III. PACKET RECEPTION RATE

When the strength of data signal is sufficiently above the noise and interference data packets can be successfully received and decoded. However, as the transmission power of the RF waves is significantly higher and because the power contained in the energy signal may leak into adjacent data communication channel, interference and packet losses may occur if this transfer occurs at different frequencies.

- *PRR and frequency.* Figures 1a and 1b present the average PRR as a function of varying ET frequencies indoor and outdoor, respectively. The data communication frequency is centered at 915 MHz. The experiments show that three distinct regions occur: In the middle region of the graph, there is the band of *black* frequencies, in which none of the packets that are transferred between sensor motes are successfully received. In these *black* frequencies, the power of energy signals that leaks into the data channel is high enough to completely block all data communications. We observe that the actual frequency range of *black* region depends on the distance of ET from the receiver (Fig. 1). More specifically, the spread of the *black* frequency region for the ET with distance of 1m is 2 MHz; for the ET

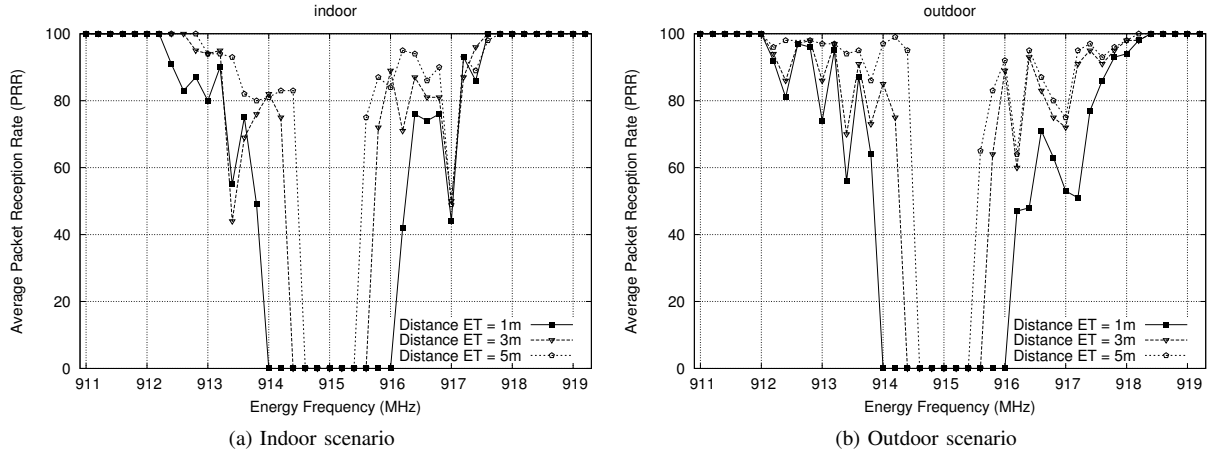


Fig. 1: Effects of varying wireless ET frequencies on PRR (a) indoor and (b) outdoor.

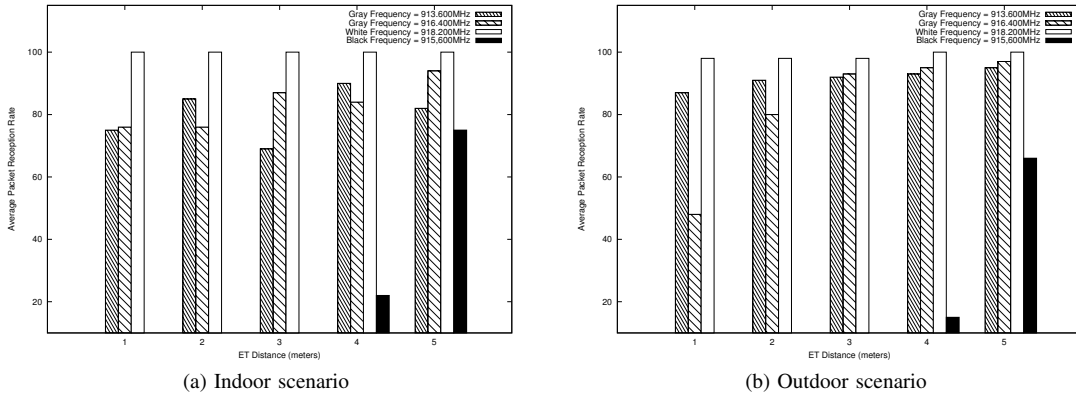


Fig. 2: Effects of ET distance on the PRR at gray, white, and black energy frequencies (a) indoor and (b) outdoor.

with distance 3m is 1.2 MHz. Similarly, for the ET with distance 5m it is 0.8 MHz. Fig. 1 shows that even when the ET is 5m away from the mote, which is the maximum effective charging range in our testbed, there are still energy frequencies with 100% packet loss. Thus, an appropriate separation of energy and data channels must be chosen in the design of protocols for such RF powered nodes.

On the extreme ends of the plots there are two frequency regions where the PRR is always uniformly high. We call these regions *white* areas, where the sensor motes experience correct reception even in the presence of concurrent wireless energy transfer from the ET. We observed that the *white* range for indoor environment includes all energy frequencies higher than 917.600 MHz and lower than 912.200 MHz (Fig. 1a). As shown in Fig. 1b, the *white* outdoor range includes those frequencies that are higher than 917.800 MHz and lower than 912 MHz. ET placement does not appear to affect the extent of the *white* region. These results further show that frequency separation is a better approach for sensor survival of energy interference and to boost network throughput, compared to duty-cycle based approaches.

Finally, we observe that both indoor and outdoor there are frequency ranges where the PRR is rather unstable. These energy frequency regions are the *gray* areas. In these, the motes experience variations in PRR ranging from 50% to 90%. While the high power of energy transfer at gray frequencies still leaks into the data channel, the energy interference has a power that is nearly the one of the data signal at the receiver. The pattern of fluctuations depends on the environment and on the form of energy signal. Interestingly, we observed that outdoor the patterns of fluctuations are symmetric for different ET distances. Indoor, however, even when multi-path fading and shadowing are limited, the reflections due to the walls resulted in different constructive and destructive interference levels at the receiver. As a consequence, for indoor environments we observe asymmetric variations of packet reception with varying ET distances. Furthermore, our measurements show that the spread of the *gray* region in both indoor and outdoor depends on the location of ETs. In particular, as the distance of ET increases, the width of the *gray* region also increases: When the ET is 1m away, the *gray* region is the narrowest; when the ET is 5m away, it is the widest.

- *PRR and distance.* Fig. 2 compares the PRR for five different ET distances for a mix of *gray*, *black*, and *white* frequency regions, both indoor and outdoor. First, we observe that the energy frequency of 915.6 MHz is within the *black* area when the ET is 1, 2, and 3 m away from the motes. As the distance increases (4 and 5 m), this frequency moves to the *gray* area. This observation highlights the importance of ET location in RF transfer frequencies assignment. We also observed that the indoor PRR at the gray frequencies does not improve monotonically for increasing distances of the ET. This is because of small reflections of energy signals. For example, at the *gray* frequency of 913.600 MHz, the PRR is lower when ET is 3 m away that when it is 2 m away. Outdoor, instead, packet reception improves monotonically with increasing distances of the ET.

Overall, our experimental study reveals that the existence and width of the three regions has important implications for RF energy harvesting-based WSNs. In particular, we have observed that the frequency of energy and data signals need to be separated beyond a threshold that depends on the distance of the ET from the nodes to allow packets to be received successfully. The naming for white, gray, and the white areas is inspired from earlier works observing similar behaviors for classical sensor networks [9], which are concerned only on inter-nodal spatial distance. In this work, the demonstrated areas refer to frequency domain in RF energy harvesting sensor networks.

IV. ENERGY INTERFERENCE

In traditional WSNs, the RSSI provides an indication of connectivity, aids access points selection, and is used to determine error-prone wireless links. However, it is not immediately obvious how the interferer power measured by the sensor nodes could be used to determine the energy frequency regions and preferred power transfer frequencies in RF harvesting WSNs. In this section, we aim at studying how knowing the distributions of the energy interference strength can be used by a node to detect in which region (*white*, *gray* or *black*) is the node, and the appropriate energy transfer channels it can use.

- *RSSI distributions with frequency.* Figures 3 and 4 illustrate the impact of different energy frequency regions on the distribution of the received interferer power indoor and outdoor, respectively. The y-axis corresponds to the RSSI values in dBm measured by the CC1000 radio of the Mica2 mote. The distance between the ET and the motes is 1 m. We also present the signal strength distribution of the ambient noise and of the data signal both indoor and outdoor, measured in absence of energy transfer. The rightmost distribution shows the RSSI of data signal (around -49 dBm), and the leftmost one shows the measured ambient signal distribution (between -93 dBm and -89 dBm) indoor. The outdoor noise is between 91 dBm and -75 dBm. Figures 3 and 4 show that the RSSI of the recorded energy can be clustered into three

ET Frequency	Outdoor			Indoor		
	Mean RSSI	StdV	PRR	Mean RSSI	StdV	PRR
918,200	-87.069	0.010	98%	-88.534	0.011	100%
918,00	-86.683	0.012	94%	-89.444	0.012	100%
917,600	-78.476	0.010	86%	-88.534	0.011	100%
916,200	-65.785	0.006	47%	-67.737	0.009	42%
915,600	-54.283	0.001	0%	-55.219	0.001	0%
915,200	-48.550	0.001	0%	-49.187	0.001	0%
914,600	-55.607	0.001	0%	-55.953	0.001	0%
914,200	-61.602	0.001	0%	-59.236	0.001	0%
913,600	-79.864	0.010	87%	-75.355	0.005	75%
912,600	-85.364	0.009	97%	-79.872	0.008	83%
912,200	-79.472	0.022	92%	-86.414	0.010	100%
911,800	-87.617	0.011	100%	-91.473	0.010	100%

TABLE I: Map of energy interference power and associated PRR.

classes corresponding to three different frequency areas. We observe a correlation between the frequency separation of energy and data and the clusters. However, within each cluster this correlation does not necessarily hold. The RSSI distributions of *black* regions are close to each other and can be clustered with the data signal, while the distributions of *white* region can be clustered with the ambient noise. The cluster for the *gray* region is in the middle. We notice that the *gray* area exhibits a wider range of RSSI than that of the other two regions.

The range of the interferer signal strength for the gray region vary from -87 dBm to -65 dBm indoor, and from -84 dBm to -64 dBm outdoor. In this region, the RSSI samples are normally distributed and can be categorized into three groups: High, medium, and low. The first group includes ET frequencies such as 916.200 MHz that exhibits higher RSSI, and hence lower packet reception rates. The second group contains frequencies such as 913.600 MHz indoor and as 912.200 MHz outdoor showing slightly lower RSSI. Finally, the third group in the gray area corresponds to ET frequencies with negligible energy interference.

The recorded RSSI at each energy transfer frequency within the *gray* area have different variances. Some ET frequencies can cause higher variations of RSSI (i.e., 912.200 MHz outdoor), while frequencies like 913.600 MHz have low RSSI variations. Comparing the two figures, we find that the RSSI values in the *gray* area exhibits markedly different patterns indoor and outdoor. For example, the indoor ET frequency 912.600 MHz has higher interferer power compared to 917.600 MHz. These power values are lower outdoor. It is shown that the *black* frequency range (rightmost point of the plots) shows a large spike of received power both indoor and outdoor, but the interference patterns remain the same. The RSSI distributions reveal that the energy interference at the *white* frequencies in both indoor and outdoor environments are negligible. This confirms the high values of PRR shown in Section III.

Table I summarizes the energy interference power and associated PRR for different ET frequencies from all regions in both indoor and outdoor environments, and strongly suggests that the measurement of energy interference within the sensor node can be used as a good estimate to detect

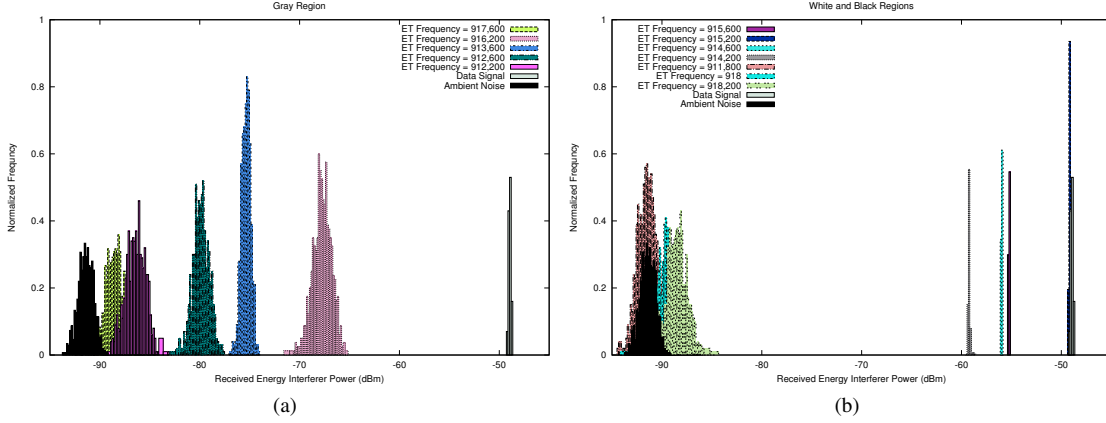


Fig. 3: Distribution of RSSI for energy interference indoor for varying ET frequencies in *gray*, *white*, and *black* regions.

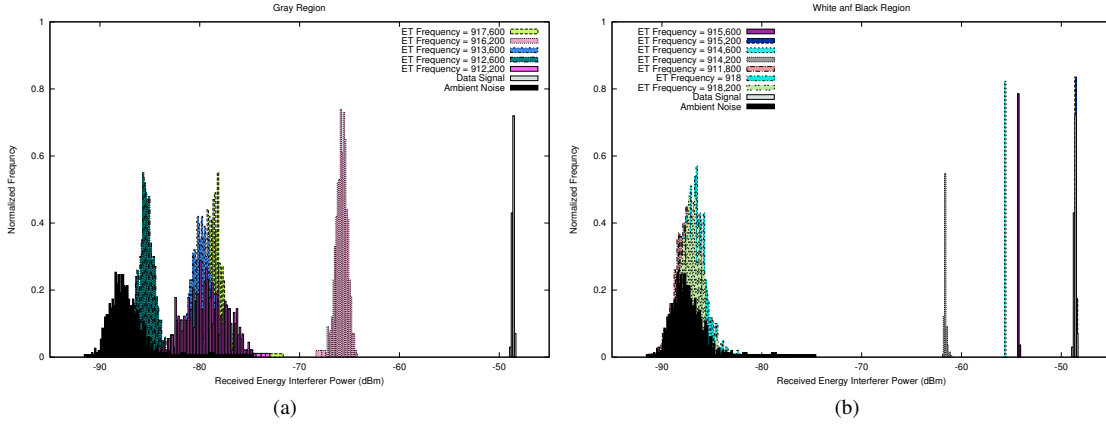


Fig. 4: Distribution of RSSI for energy interference outdoor for varying ET frequencies in *gray*, *white*, and *black* regions.

energy areas and appropriate energy frequencies in RF harvesting sensor networks.

- *RSSI and distance.* We investigate the relationship between the distance among ET and motes, and the RSSI at the receiving mote. We plot the received interferer power for varying distances and energy frequency regions both indoor and outdoor. Due to space limitations, we show results for the *gray* frequency (913.600 MHz) indoor (Fig. 5a) and outdoor, and for the *white* frequency (911.800 MHz) regions outdoor only (Fig. 5b).

In Figure 5a, we see that the interference may increase with increasing ET distance. Specifically, the measured RSSI for ET located at distance 1m is about -76 dBm, however, the RSSI increases to about -74 dBm at distance 3m. This occurs because of reflections in the indoor setup, and confirms the asymmetric PRR variations over different ET distances. In outdoor environment, the received interferer power decreases as the distance of ET increases. In particular, Figure 5b shows that the measured power is about -80 dBm for ET distance 1m, and it decreases to about -84 dBm and -87 dBm for ET distances 3m and 5m, respectively. Thus, the distribution of energy interference

at the *white* frequency region has very few changes with the location of the ET. Our measurements indicate that both gray and white frequencies have normal interference distributions over all ET distances.

V. TEMPORAL CHANGE IN ENERGY INTERFERENCE

In this section, we examine how the energy interference varies with time for indoor and outdoor environments.

Figure 6 shows the received energy interferer power for the three colored frequency regions at different ET distances of 1m, 3m, and 5m. The energy interference when ET transfers at the *gray* frequency region shows significant variations over time in the outdoor environment. On the other hand, the indoor scenario that caused noticeable variations in RSSI compared to the ambient noise, exhibits comparatively less temporal variation. The high temporal variation results indicate not only sensor nodes experience variable PRR over different gray frequencies, but also the fact that nodes experience time varying energy interference at each frequency. In addition, these results suggest to continuously measure the energy interferer power at gray frequencies since the RSSI can vary significantly over time. Figures 6c and 6d show the temporal variations in the

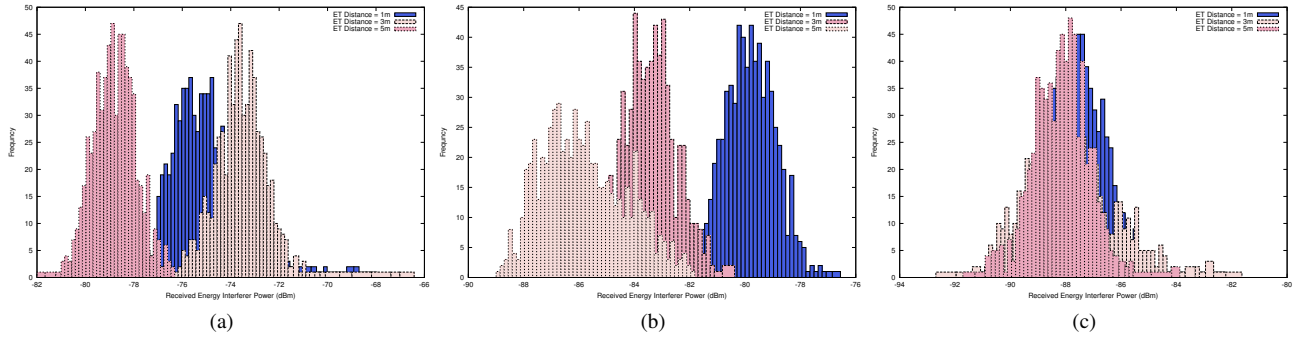


Fig. 5: Effects of different ET distances on distributions of energy interference for (a) indoor gray region, (b) outdoor gray region, and (c) outdoor white region.

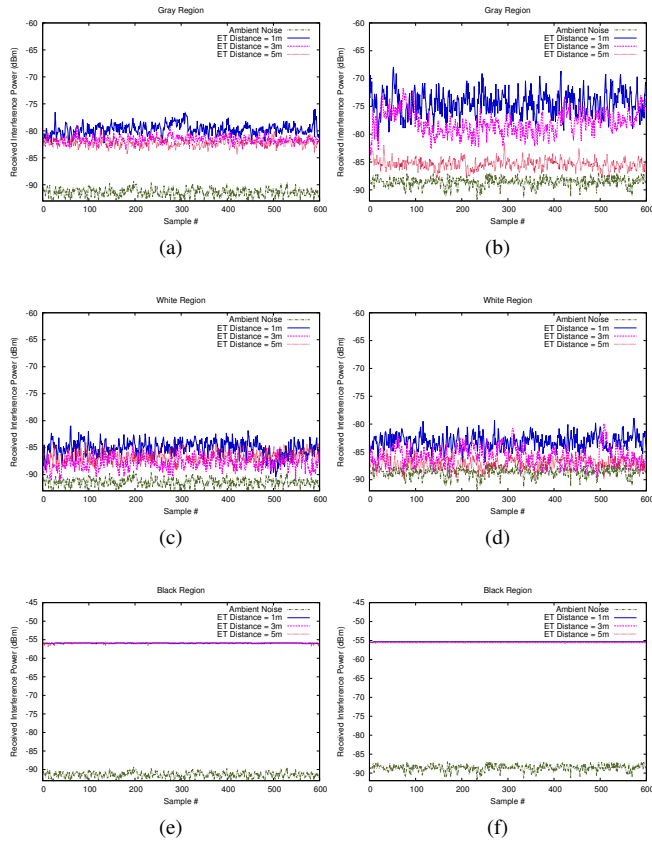


Fig. 6: Temporal characteristics of energy interference power in indoor (a, c, e) and outdoor (b, d, f) environments for gray, black, and white frequency regions.

white region, which is comparatively less than those in the gray region. The interference caused by energy transfer in the black frequency band caused no variations in the measured RSSI. Interestingly, in all the plots, we find that the variation of the interferer power decreases as the distance between ET and the sensor node increases.

VI. CONCLUSIONS

We presented an experimental study to understand the effect of RF energy transfer from an energy transmitter

on low-power data communications, as those of WSNs. Our results confirm that multifrequency energy transfer is crucial for surviving energy interference and improving the PRR. We discovered three distinguishable regions in the frequency domain, each of which results in different levels and pattern of interference. Finally, we showed that local energy interference measurements at a sensor node can provide a good estimate for detecting the energy frequency regions where the node is, thus guiding the selection of ET frequencies for a desirable PRR.

ACKNOWLEDGMENTS

This work was supported in part by the US National Science Foundation under research grants CNS-1143681.

REFERENCES

- [1] Powercast, <http://www.powercastco.com>, 2013.
- [2] S. Basagni, M. Y. Naderi, C. Petrioli, and D. Spenza, "Wireless sensor networks with energy harvesting," in *Mobile Ad Hoc Networking: Cutting Edge Directions*, S. Basagni, M. Conti, S. Giordano, and I. Stojmenovic, Eds. Hoboken, NJ: John Wiley & Sons, Inc., March 5 2013, ch. 20, pp. 703–736.
- [3] "Powercast P2110 powerharvester datasheet," 2013. [Online]. Available: <http://www.powercastco.com/PDF/P2110-datasheet.pdf>
- [4] P. Nintanavongsa, U. Muncuk, D. Lewis, and K. Chowdhury, "Design optimization and implementation for rf energy harvesting circuits," *IEEE Journal on Emerging and Selected Topics in Circuits and Systems*, vol. 2, no. 1, pp. 24–33, March 2012.
- [5] D. Yang, Y. Xu, and M. Gidlund, "Wireless coexistence between IEEE 802.11- and IEEE 802.15.4-based networks: A survey," *Int. Journal of Distributed Sensor Networks*, vol. 2011, pp. Article ID 912 152, 17 pages, 2011.
- [6] L. Angrisani, M. Bertocco, D. Fortin, and A. Sona, "Experimental study of coexistence issues between IEEE 802.11b and IEEE 802.15.4 wireless networks," *IEEE Trans. on Instrumentation and Measurement*, vol. 57, no. 8, pp. 1514–1523, 2008.
- [7] K. R. Chowdhury and I. F. Akyildiz, "Interferer classification, channel selection and transmission adaptation for wireless sensor networks," in *Proceedings of IEEE ICC 2009*, 2009, pp. 1–5.
- [8] V. Gungor, B. Lu, and G. Hancke, "Opportunities and challenges of wireless sensor networks in smart grid," *IEEE Trans. on Industrial Electronics*, vol. 57, no. 10, pp. 3557–3564, 2010.
- [9] J. Zhao and R. Govindan, "Understanding packet delivery performance in dense wireless sensor networks," in *Proceedings of ACM SenSys 2003*, 2003, pp. 1–13.
- [10] K. Srinivasan, P. Dutta, A. Tavakoli, and P. Levis, "An empirical study of low-power wireless," *ACM Trans. on Sensor Networks*, vol. 6, no. 2, pp. 16:1–16:49, March 2010.